Appl. Chem. Eng., Vol. 28, No. 1, February 2017, 125-131
https://doi.org/10.14478/ace.2017.1001

Article

공기와 물이 형성하는 계면에서 발생하는 유기적으로 기능화된 은 나노 입자들의 2차원 조립

정성욱

부산대학교 공과대학 화공생명공학부
(2017년 1월 6일 접수, 2017년 1월 11일 심사, 2017년 1월 12일 채택)

Two-dimensional Assembly of Organically Functionalized Ag Nanoparticles at Air-water Interface

Sungwook Chung

School of Chemical and Biomolecular Engineering, Pusan National University, 2, Busandaehak-ro 63beon-gil, Geumjeong-gu, Busan 46241, Korea
(Received January 6, 2017; Revised January 11, 2017; Accepted January 12, 2017)

초 록

본 연구에서는 유기적으로 기능화된 은 나노 입자들은 공기와 물이 형성하는 계면에서 자발적 조립 과정을 통해 새로운 2차원 상부 구조들(superstructures)을 생성하는 것을 발견하였다. 상부 구조의 분석은 금속 나노 입자의 심형과 입자 계면에 결합된 유기 분자의 크기를 바꿈으로써 입자 간 특징적 상호 작용(characteristic inter-particle interaction)을 조절할 수 있고 이들 사이의 미묘한 상호 작용(subtle interplay)을 통해 은 나노 입자의 2차원 조립이 발생함을 시사한다. 본 연구를 통해 발견한 새로운 구조들은 기능성 나노 소재, 촉매 및 소자 응용 분야에 매우 중요한 잠재적 용도가 있을 것이라 사료된다.

Abstract

We report organically functionalized Ag nanoparticles spontaneously form two-dimensional (2D) novel superstructures at the air-water interface. Analysis of the superstructures suggests that the 2D assembly of Ag nanoparticles originates from a subtle interplay between characteristic inter-particle interactions that can be readily controlled by changing the sizes of nanoparticle metal core and surfactants. Such structures have potential uses in nanostructured functional materials, catalysis, and device applications.

Keywords: *Ag nanoparticles, self-assembly, interfaces, Langmuir-Blodgett films*

1. Introduction

Phase separated structures occur in many different single- and multi-component condensed phase materials over various length scales and are driven by a variety of mechanisms. Microscopically such separations result in the formation of structures, such as lamella or granular phases, with a degree of periodicity or a characteristic length scale. In three-dimension (3D), typical examples are binary metal alloys which form eutectic mixtures[1,2], bimodal colloidal suspensions[3], diblock copolymers[4,5], and other binary combinations of polymers, colloids, and liquid crystals. In two-dimension (2D), such phenomena have been observed at the air-water and solution-solid interfaces of the Langmuir and self-assembled monolayers of binary mixtures[6-9]. A phase separation in these 2D systems typically leads to interesting periodic structures[10-13].

The origin of phase separation can be attributed to kinetically or thermodynamically controlled processes. For example, a phase separation of the metal alloy is presumed to occur via a kinetically controlled process at the front of a solidifying liquid mixture, and it is confirmed in computer simulations[14]. Evaporation of thin films of nanocrystal solution have shown phase separated spatial patterns in 2D, which is also suggested to occur via a kinetically controlled process due to increased van der Waals interactions between nanocrystals[15,16]. On the other hand, the nature of phase separation is governed by thermodynamically controlled processes which are favored entropically[17] or energetically[18]. The former is the separation of the droplets having

† Author: Pusan National University,
School of Chemical and Biomolecular Engineering, 2, Busandaehak-ro 63beon-gil, Geumjeong-gu, Busan 46241, Korea
Tel: +82-51-510-2397 e-mail: sungwook.chung@pusan.ac.kr

pISSN: 1225-0112 eISSN: 2288-4505

different sizes from uncharged bimodal oil emulsions in water, and the latter is the case of polymer blend films where a minimum energy is achieved through the separation of the components.

Organically functionalized metal nanoparticles are excellent candidates for studying the phase separation processes in 2D environments. First of all, most of the studies of macromolecular systems that show phase separated phenomena are typically limited to the structures of which the length scale of their domains are in the micron or larger due to the minuscule size of their molecular building blocks and their relatively strong and short-ranged interactions. Considering the slightly larger size and longer-ranged dispersion interactions of metal nanoparticles, organizing metal nanoparticles in 2D is likely to produce superstructures with a length scale of a sub-micron or even a smaller one. Second, direct visualization of these particular phases down to a single molecule resolution is rather a difficult task. Metal nanoparticles allow us to observe superstructures that are the outcome of the phase separation with an enhanced visibility because of high image contrast obtained from electron microscopy or scanning probe microscopy. Third, the spherical symmetry of such metal nanoparticles makes the efforts of modeling the inter-particle interactions relatively easier to explain the phase behavior than that of macromolecular complexes.

Many approaches utilizing self-assembly have emerged as powerful techniques for controlling the structure and properties of nanoparticle superstructures[19]. One of the approaches is to use Langmuir-Blodgett (LB) techniques to organize nanoparticles and nanowires at the air-water interface[20]. Herein we present results from non-templated spontaneous patterning phenomena of organically functionalized Ag nanoparticles (NPs) at the air-water interface. When building blocks are organized into an ordered structure, the shape of the building blocks often influences the symmetry of the resulting superstructure[21]. If the building blocks were Ag NPs that have a spherical symmetry, one would predict that they would readily form hexagonal close-packed (HCP) structures when they were packed together in 2D. Surprisingly we have discovered novel 2D superstructures assembled from Ag NPs, in addition to one with simple HCP symmetry, formed at the air-water interface via *ex-situ* transmission electron microscopy (TEM). By preparing the LB films of Ag NPs with varying the number ratio between two types of Ag NPs at different surface pressures of the LB isotherms, we were able to analyze novel 2D superstructures resulting from three separate cases : (Case I) type I Ag NPs with a large Ag metal core with relatively short surfactants; (Case II) type II Ag NPs with a small Ag metal core with relatively long surfactants; (Case III) a mixture of both type I and II Ag NPs. Each case has characteristic inter-particle interactions that can be readily controlled by varying the sizes of Ag NP metal cores and surfactants.

2. Experimental

2.1. Synthesis of Ag NPs.

The synthesis of size-selected 4~5 nm diameter dodecanethiol-capped Ag NPs was developed elsewhere[22-25]. An amount of either $AgNO_3$ or $AgClO_4$ was dissolved in Nanopure H_2O. The aqueous Ag salt solution was then quantitatively transferred into either toluene or chloroform using tetraoctylammonium bromide ($(C_8H_{14})_4NBr$) as a phase transfer reagent under vigorous stirring. Octanethiol ($C_8H_{17}SH$), dodecanethiol ($C_{12}H_{25}SH$), and octadecanethiol ($C_{18}H_{37}SH$) were used as alkanethiol surfactants for the synthesis. Typically a measured amount of ~10 mmol alkanethiol was added to the aqueous-organic mixture. In a separate container, a measured amount of $NaBH_4$ reducing agent was dissolved in Nanopure H_2O. While the Ag-containing mixture was rapidly stirred, the aqueous solution of $NaBH_4$ was added slowly to the mixture and the reaction was allowed to proceed for ~12 h. For the case of toluene solvent synthesis, a typical molar ratio for $AgNO_3/(C_8H_{14})_4NBr/alkanethiol/NaBH_4$ was ~1 : 1 : 5 : 10 and a typical amount of initial Ag salt reagent was 400 mg (2.35 mmol). For chloroform solvent synthesis, the molar ratio of reagents was ~1 : 3 : 3 : 10. It was found that relatively larger sizes (> 5 nm) of Ag NPs with narrower size distributions were produced from the chloroform synthesis. Upon completion of the reaction, the aqueous layer was removed and the organic layer was rotary evaporated to a volume of ~5 mL. Ag NPs were precipitated from the organic portion by adding polar solvents such as methanol or acetone and cooling to -25 ℃ in the freezer for ~12 h.

The initial size distribution was often broad and could be narrowed using the technique of size-selective precipitation[23,26]. The majority of Ag NPs used here was size-selectively precipitated at least three times.

2.2. Preparation of Langmuir-Blodgett (LB) films of Ag NPs.

Following synthesis and size selection, Ag NPs were ligand exchanged with shorter or longer surfactants (such as linear chain alkanethiol molecules with different sizes) if needed and re-precipitated. Typically ligand exchange was performed by adding 1 mL of ~5 mg/mL Ag NP solution (Ag NPs dissolved in nonpolar organic solvents such as hexane or toluene) to a solution of hexane containing an excess of the desired alkanethiol (~10 mmol) under vigorous stirring for 10 min. Ligand exchanged Ag NPs were then purified by centrifugation after adding acetone as a flocculent agent. More than 96% (molar ratio) of the as-synthesized Ag NPs were ligand exchanged through this process.

The product (dark green powder) was dispersed by water bath sonication in an acetone/methanol solution and filtered in order to remove any residual organic surfactant. The resulting dry powder was weighed and dissolved in a known amount of chromatographic grade hexane, heptane or chloroform to a concentration of ~1 mg/mL. The maximum solubility of Ag NPs in hexane is about ~25 mg/mL depending on NP size, alkanethiol surfactants, and previous chemical treatments. Finally, the Ag NP solution was passed through a 0.2 μm pore size membrane filter to remove both undissolved precipitates and excess unbound organic alkanethiol surfactants and the final Ag NP solution was used immediately within 10 minutes.

LB films of the Ag NPs were formed on a Nima Technology Type 611 Langmuir trough with typically ~1 mg/ml solution of Ag NPs in hexane, heptane, or chloroform. Temperature is mostly held constant

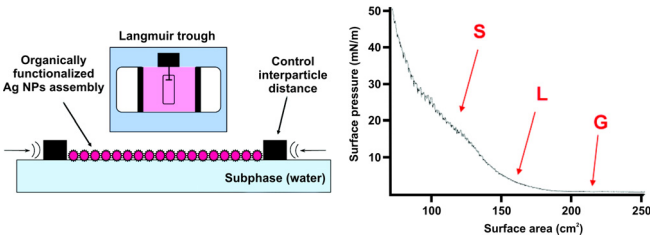

(A) (B)

Figure 1. (A) Experimental diagram of preparing the LB films of Ag NPs on a Langmuir trough. (B) Typical pressure-area (π-A) Langmuir isotherm of the LB films of Ag NPs. Note that "S" indicates the solid phase, "L" liquid, and "G" gaseous phase of the LB films of Ag NPs.

(~15 ℃) throughout the experiment. In most experiments, one drop (~3 μL volume) of Ag NP solution was placed on the water surface. The resulting LB films were transferred to various substrates such as carbon-coated grids, mica, or silicon wafers via Langmuir- Schaeffer (i.e. horizontal liftoff) technique. This type of transfer has been previously shown to be very effective at transferring Langmuir monolayers of quantum dots and nanowires[20].

Ex-situ TEM (120 keV Philips model CM120 TEM and 200 keV Akashi high-resolution TEM) was used to characterize the LB films of Ag NPs. The approximate number density of Ag NPs on the water surface depends strongly on the concentration of Ag NP solution from which they were taken for the single drop experiment. Usually, only a small fraction of the water surface remained covered by islands of the monolayer film of Ag NPs after solvent evaporation. Due to the intense optical signature that is characteristic of Ag NPs, a surface coverage of even sub-monolayer films could often be observed by naked eye. An alternative technique was used to deposit a few drops to *fill up* certain area fraction on the Langmuir trough. Here, fill up does not mean a full monolayer coverage but rather a similar coverage as was observed locally for the single drop case. Then, compressing the LB films of Ag NPs changed the number density of Ag NPs in the LB films on the Langmuir trough. Figure 1A shows a graphical illustration of the experiment using the Langmuir trough on which Ag NP film is formed on the water surface. Figure 1B is a typical pressure-area (π-A) isotherm of the LB film of Ag NPs. Usually, samples were taken at different surface pressures or Ag NP concentrations and then investigated by *ex-situ* TEM.

3. Results and Discussion

It has been reported that size-dependent dispersion interactions play a critical role in the metal NP assembly[23]. The ratio of the inter-particle distance (D) between the NPs to the size of the metal core ($2R$, R is the radius of the metal core) $D/2R$ is the critical physical parameter for determining the nature of the dispersion attraction between metal NPs. For our system, D is mostly determined by the length (L) of the alkanethiol surfactants attached to the metal core of Ag NPs. Therefore, we chose two circumstances - Ag NPs of a large metal core with relatively short surfactants and a small metal core with relatively long surfactants in order to investigate the role of inter-particle interactions for 2D Ag NP assembly at the air-water interface. Also, we investigated the third case of incorporating both types of Ag NPs for 2D Ag NP assembly.

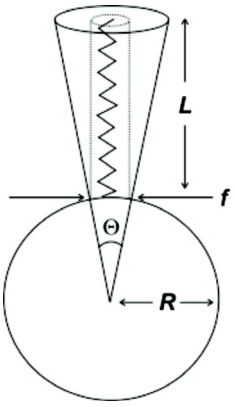

Figure 2. Illustration of an excess volume (V_e) available to the organic surfactant of the metal NP with the radius (R) of the metal core[23]. The angle (Θ) defined in the cone is determined by the footprint size (f) of each organic surfactant and R of the metal core.

3.1. Case I : type I Ag NPs with a large metal core with relatively short surfactants.

In Case I, the basic unit of the assembly is Ag NP with a large metal core with relatively short surfactants, which is entitled as type I Ag NP. Figure 2 shows an illustration of Ag NP showing a concept of excess volume (V_e) defined by the parameters such as D and $2R$ previously[23]. V_e is the free volume of a hollow cone available to the organic surfactant as it extends from the surface of a spherical metal NP. This volume scales as $\frac{L^3}{R^2}$ which gives an idea of how much the surfactant shell volume of one NP may interfere with that of another NP. If two Ag NPs are brought together in the vicinity of each other, their surfactant shells start to penetrate. Such penetration of the surfactant shells will allow the maximum dispersion attractions between the shells of type I Ag NPs.

For the case of type I Ag NPs, R of the metal core is considerably larger than L of the surfactants. In our experiment, Ag NPs have 4~6 nm diameter metal core with relatively short alkanethiol surfactants such as octanethiol ($C_8H_{17}SH$), which provides with approximately ~ 0.9 nm of L and their V_e corresponds to ~5.0×10^{-2} nm^3. If V_e remains between 5.0×10^{-2} nm^3 and 3.0×10^{-1} nm^3, which falls in the category of type I, there are only three existing phases of 2D Ag NP assembly in the LB films: 1) compressible gaseous phase, 2) condensed, close-packed 2D phase, and 3) collapsed multilayer 3D phase according to the phase diagram reported in the literature[23]. In terms of compressible gaseous phase, it was discovered not to be gas-like at all, but has the 2D superstructures of *circular domains* and *stripes* composed of type I Ag NPs[27,28]. Figure 3 is TEM micrograph of *intermediate* phases of an array of circular domains (Figure 3A) at almost

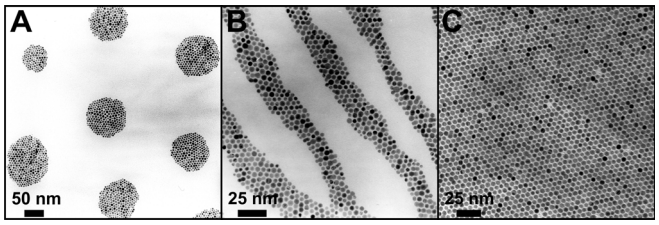

Figure 3. TEM micrographs of an array of circular domains, stripes, and HCP domains assembled from type I Ag NPs in the LB films : (A) Circular domains of ca. 6 nm diameter octanethiol-capped Ag NPs at almost zero surface pressure (π ~0 mN/m). (B) Stripes of the same Ag NPs at low surface pressure (π ~1.5 mN/m). (C) HCP domain of the same Ag NPs at high surface pressure (π ~10 mN/m).

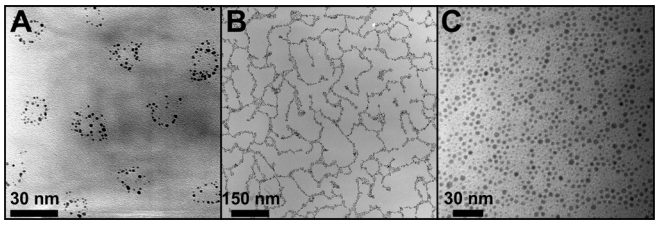

Figure 4. TEM micrographs of an array of ring-like domains, low compression NP foam, and high compression NP foam assembled from type II Ag NPs in the LB films : (A) Ring-like domains of ca. 3 nm diameter octadecanethiol-capped Ag NPs at almost zero surface pressure (π ~0 mN/m). (B) Space-filling, low compression NP foam of the same Ag NPs at low surface pressure (π ~5 mN/m). (C) Extended, high compression NP foam of the same Ag NPs at high surface pressure (π ~20 mN/m).

zero surface pressure (π ~0 mN/m) and an array of stripes (Figure 3B) at low surface pressure (π ~1.5 mN/m). As the surface density of type I Ag NPs in the LB films increased, type I Ag NPs aggregated into the circular domains at the surface coverage of ~20% and then the circular domains were transformed to stripes at the surface coverage of ~50%. As the stripes were fully compressed in the LB films, they were converted into a continuous, HCP array of Ag NPs. Figure 3C shows the HCP array of Ag NPs at high surface pressure (π ~10 mN/m) before the point of monolayer collapse in the LB films. These HCP domains of type I Ag NPs were typically extended up to a few tens of micrometers showing a long-ranged order.

3.2. Case II : type II Ag NPs with a small metal core with relatively long surfactants.

In Case II, the basic unit of the assembly is Ag NP with a small metal core with relatively long surfactants, which is entitled as type II Ag NP. In this case, R of the metal core of the NP is considerably smaller than L of the surfactants. In our experiment, type II Ag NPs typically have 2~3 nm metal core diameter with relatively long surfactants such as octadecanethiol ($C_{18}H_{37}SH$) with L of approximately ~2.0 nm. Therefore, V_e of type II Ag NPs corresponds to 0.5~1.5 nm^3. It has shown that type II Ag NPs at the air-water interface led to compressible, extended, low-density 1D phase structures[23]. Surprisingly, one of the 2D superstructures from the low-density 1D phase turned out to be an array of *ring-like domains* assembled from type II Ag NPs. Figure 4A shows the array of ring-like domains that have an arrangement of a pearl necklace at almost zero surface pressure (π ~0 mN/m). It is interesting to note that the majority of ring-like domains appeared to have an annulus of almost single NP or so.

There is a significant resemblance between the ring-like domains of type II Ag NPs (Figure 4A) and the circular domains of type I Ag NPs (Figure 3A). Despite the similarity in their shape and curvature, the average diameter of the circular domains assembled from type I Ag NPs was slightly greater than that of the ring-like domains assembled from type II Ag NPs. Furthermore, type II Ag NPs appeared to have just a few neighboring NPs within the annulus of the ring-like domains while type I Ag NPs to have the HCP arrangement by maximizing the number of neighboring NPs within the circular domains. Having only a few neighbors around type II Ag NPs in the ring-like structures suggests that the nature of interactions between type II Ag NPs are likely to be anisotropic and directional rather than isotropic.

Figure 4B is TEM micrograph of type II Ag NPs assembled into a *percolating network* of NPs at intermediate surface pressure (π ~5 mN/m). This network has been referred as a *foam* structure composed of Ag NPs[23]. Note that the fraction of the void area within the Ag NP foam is more than 60~80% and some branches of the foam network tend to be bent. These characteristics suggest a highly compressible phase behavior of Ag NP foam with a substantial mechanical flexibility. Indeed, upon further compression of the LB film of Ag NP foam to a high surface pressure (π ~20 mN/m), an *extended space-filling network*, or a higher density of Ag NP foam, was obtained. Figure 4C is TEM micrograph of the higher density foam structure composed of type II Ag NPs. Ag NP foams with both intermediate (π ~5~10 mN/m) and high compression (π ~20 mN/m) maintained their framework of a percolating network over a length scale of approximately one micrometer while the fraction of the void area with higher compression was slightly smaller than that with intermediate compression. It is worth addressing that Ag NP foams with both intermediate and high surface pressure showed a similar preference of accommodating mostly 2-fold and 3-fold coordination of the neighboring Ag NPs.

The microscopic origin of the interaction that leads to the percolating network of Ag NP foam has not been fully understood. However, a phenomenological analysis based on the model of excess volume[23] shown in Figure 2 was used to rationalize the formation of Ag NP foam. When two type II Ag NPs are brought together, their surfactants start interpenetrating the surfactant shell, which leads to a distortion of the shell constituting the excess volume. If a third type II Ag NP approaches, it will interact with the pair of type II Ag NPs by establishing a three-body interaction in a highly directional manner. Allowing this three-body interaction would maximize the net attractive dispersion interaction via interpenetrating the surfactant shell of three Ag NPs and allow multiple bonding sites on them. It is likely that the idea of highly directional, anisotropic interactions between type II Ag NPs may offer a clue to understanding the formation of Ag NP foam structure in the LB films. Indeed, our experimental results have shown that type

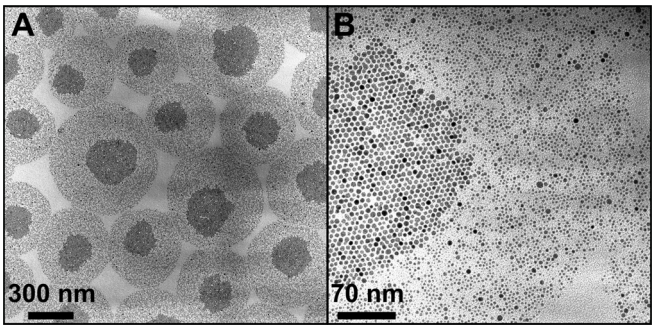

Figure 5. (A) TEM micrograph of an array of egg-like domains assembled from 1 : 1 : mixture of ca. 6 nm diameter octanethiol-capped Ag NPs (type I) and ca. 3 nm diameter octadecanethiol-capped Ag NPs (type II) in the LB films. (B) Higher resolution TEM micrograph of an individual egg-like domain that consists of an egg yolk assembled from the same type I Ag NPs surrounded by an egg white assembled from the same type II Ag NPs.

II Ag NPs initially formed the low density, ring-like domains and once compressed, they were transformed to the highly compressible, extended percolating network prior to the point of monolayer collapse at the air-water interface.

3.3. Case III : Mixture of type I and II Ag NPs

In Case III, we discovered that an array of *egg-like domains* in the LB films was spontaneously formed at the air-water interface when depositing several drops (~3 μL volume per one drop) of ~1 mg/mL Ag NP solution of which both type I and II Ag NPs coexist with approximately ~1 : 1. Figure 5A and 5B are TEM micrographs of the egg-like domains that are assembled from both type I and II Ag NPs in the LB films at low surface pressure (π ~2 mN/m). Note that the egg-like domain is consist of an *egg yolk* and *egg white*: within the individual egg-like domain shown in Figure 5B, type I Ag NPs were predominantly organized into the circular domain, which is referred as the egg yolk surrounded by a shell of type II Ag NP foam, which is referred as the egg white.

A couple of features in the egg-like structures are worth mentioning. First, all three cases favored the organization of Ag NPs towards the array of domains with a circular perimeter when they were assembled on the water surface at relatively low surface pressure. In particularly, Case III showed that type I Ag NPs from the mixture had a tendency of organizing themselves into the egg yolk with the HCP arrangement that was similarly observed when only type I Ag NPs were present. Second, type II Ag NPs from the mixture exclusively organized into the egg white showing almost perfect circular shells around the egg yolk and these shells had a very similar arrangement of the Ag NP foam created when only type II Ag NPs were present.

Aggregation of type II Ag NPs into the NP foam around the egg yolk of type I Ag NPs suggests that the egg white shell has a preference of wetting the perimeter of the egg yolk, which may decrease the total energy of the system not only by screening the longer-ranged repulsions between the circular domains but also by reducing their interfacial energy. However, it is somehow difficult to explain why the NP

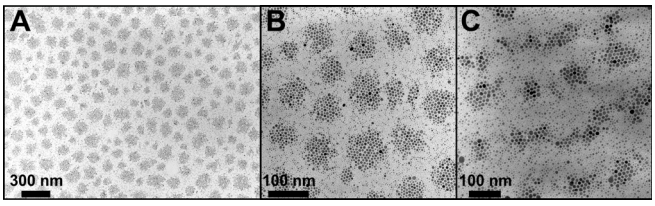

Figure 6. TEM micrographs of emerging lamellar domains assembled from the same mixture of Ag NPs described in Figure 5. (A) Initial formation of an lamellar structure via a compression of the array of the egg-like domains shown in Figure 5 at intermediate surface pressure (π ~10 mN/m). (B) Higher resolution TEM micrograph of Figure 6A. (C) Lamellar structure of the same mixture at high surface pressure (π ~20 mN/m).

foam of the egg white maintains its curvature even when it is almost in contact with other egg white shells of the neighboring egg-like domains, which is supposed to be energetically unfavorable. Based on our hypothesis that the assembly of the egg-like domains is probably not a thermodynamically controlled but a kinetically controlled process, it is likely that a significant kinetic barrier for reorganizing the overall configuration of the egg white shell may exist even when the shell is in contact with other shells.

As the LB films of the mixture were compressed, the egg-like domains were first compressed towards each other and then the egg yolks were broken and withered into smaller sizes while still surrounded by type II Ag NP foam. Figure 6A and 6B show TEM micrographs of emerging *lamellar domains* in the LB films at intermediate surface pressure (π ~10 mN/m). Figure 6C shows TEM micrograph of the very same lamellar structure at high surface pressure (π ~20 mN/m). The beginning of the evolution from the egg-like to lamellar structures is clearly visible in Figure 6A, 6B, and 6C.

If we examined the withered circular domains of the egg yolks in Figure 6A, 6B, and 6C, we uncovered that their overall configuration is reminiscent of the formation of opals from polydisperse nanoparticles[29]. The structure of the opals made from polydisperse nanoparticles illustrates the preferential arrangement of larger nanoparticles located at their center and smaller ones populated at their perimeter. The structure of the withered circular domains shown in Figure 6A, 6B, and 6C is similar to that of the opals of which their configuration is a thermodynamically favorable one. Therefore, we concluded that the compression of the LB films of the egg-like domains is likely to enhance the mixing of type I and II Ag NPs by withering down the egg yolks.

Figure 7 shows a highly compressed lamellar structure produced from the separate mixture of approximately 1 : 1 ratio of type I and II Ag NPs at even higher pressure (π ~25 mN/m). It is composed of alternating stripes of mostly one type of Ag NPs, not of the mixture. Note that there is a net diagonal alignment of stripes over a length scale of a micrometer. We think that net alignment is probably due to the compression of the LB film by two barriers of the Langmuir trough.

Lamellar structures are often observed in the systems where a phase transformation front moves quickly, leaving behind two solid products

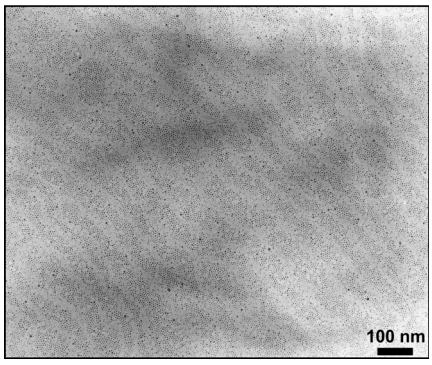

Figure 7. Low resolution TEM micrograph of a highly compressed lamellar structure assembled from the mixture of ca. 6 nm diameter octanethiol-capped Ag NPs (type I) and ca. 3 nm diameter octadecanethiol-capped Ag NPs (type II) in the LB films at high surface pressure (π ~20 mN/m).

as in the example of rapid cooling of eutectic or eutectoid systems[30]. Similar phenomena have been observed in the films of immiscible liquid mixtures at the air-water interface[31]. Thin films of self-assembled block co-polymers have been used as templates for incorporating inorganic nanoparticles into ordered nanostructures such as lamellar structures[32,33]. However, there has been almost no example of non-templated approach to the lamellar structures assembled from binary metal nanoparticles within the LB films and the discoveries of the lamellar structures in our current study is significant in this regard.

The nature of the transition from the egg-like to the lamellae of type I and II Ag NPs has not been understood well nor investigated in depth due to a slow equilibration of the compressed phases of the Ag NP LB films. Our phenomenological analysis on the transition from the egg-like to the lamellae suggests that the transition depends on the thermodynamic mixing of different types of Ag NPs that are the building blocks of the egg-like domains. If the transition were reversible, there would be a coexistence of the egg-like domains and the lamellae while being compressed. We have not been able to observe the coexistence of the egg-like and the lamellae in our experiment implying that the transition is not reversible. Instead, we discovered that the shrinkage of the egg yolks occurred gradually and the critical surface pressure required for the egg-like to the lamellae transition increased significantly when the number ratio of type I to type II Ag NPs increased. This is perhaps due to an increased difficulty of mixing type I and II Ag NPs within the array of the egg-like domains when more type I Ag NPs were present. Because of this energy penalty to pay when mixing type I and II Ag NPs, a compression process of the LB films of the egg-like domains offers an effective route to the formation of the lamellar structures assembled from binary Ag NPs.

One key question, which is often asked about when the phase separated structures with a certain periodicity are being observed, is whether they represent a true equilibrium state of the system or not. Our system is an experimental challenging one due to relatively strong and short-ranged attractions between Ag NPs, which make the observation of reversibility extremely difficult. Therefore, it is likely that 2D superstructures of our system may not represent a true equilibrium structure. Also, unlike the example of the LB films of amphiphilic molecules, which are characterized by a variety of thermodynamic phases such as gas, expanded liquid, condensed liquid, and solid, the LB films of Ag NPs have a pseudo-continuum of 2D condensed phases with a variable degree of order and fluidity[23]. Their order and fluidity are found to be a function of several experimental parameters, one of which is the ratio of the size of metal core to the length of organic surfactants attached to the metal nanoparticle. Further studies of the 2D condensed phase behaviors of Ag NP LB films and their responses to experimental parameters are still ongoing and will be reported in the near future.

4. Conclusions

Organically functionalized Ag NPs were synthesized and assembled at the air-water interface. The resulting 2D superstructures of Ag NPs in the LB films were examined as a function of the number density of Ag NPs and the surface pressure of the corresponding LB films. Three separate cases have been investigated. In Case I, type I Ag NPs having a large metal core with relatively short surfactants led to the 2D superstructure of the circular domains in the LB films at almost zero surface pressure (π ~1.5 mN/m). Once the LB films were compressed, the circular domains were transformed into the stripes at low surface pressure (π ~1.5 mN/m) and eventually the stripes were merged into the HCP domains at high surface pressure (π ~10 mN/m) prior to the point of monolayer collapse in the LB films. In Case II, type II Ag NPs having a small metal core with relatively long surfactants formed the 2D superstructure of the ring-like domains in the LB films at almost zero surface pressure (π ~0 mN/m) and then they were evolved into the extended, percolating network, known as the Ag NP foam structure, when they were compressed at intermediate surface pressure (π ~5 mN/m). Once they were fully compressed prior to the point of collapse, they formed the highly compressed Ag NP foam structure at high surface pressure (π ~20 mN/m). In Case III, when almost an equal amount of type I and II Ag NPs were mixed in the LB films, they spontaneously formed the egg-like domains in the LB films at low surface pressure (π ~2 mN/m). Eventually, they were transformed into the lamellar structures that are composed of the alternating array of the stripes of type I and II Ag NPs as the LB films were fully compressed to high surface pressure (π ~25 mN/m).

Although the nature of the 2D assembly process of Ag NPs at the air-water interface has not been entirely comprehended, we attribute the formation of their 2D superstructures to their characteristic inter-particle interactions that can be readily controlled by varying the sizes of NP metal cores and surfactants. In the end, our study provides with a structural map of 2D Ag NP assembly and the map reveals enriched structural information of unique 2D superstructures of Ag NP assembly at the air-water interface.

Acknowledgements

This work was supported by a 2-Year Research Grant of Pusan National University.

References

1. R. Kerridge, 890. Melting-point diagrams for binary triglyceride systems, *J. Chem. Soc.*, 4577-4579 (1952).
2. A. A. Wheeler, W. J. Boettinger, and G. B. Mcfadden, Phase-field model for isothermal phase-transitions in binary-alloys, *Phys. Rev. A*, **45**, 7424-7439 (1992).
3. S. Jamali, M. Yamanoi, and J. Maia, Bridging the gap between microstructure and macroscopic behavior of monodisperse and bimodal colloidal suspensions, *Soft Matter.*, **9**, 1506-1515 (2013).
4. R. Koningsveld, W. H. Stockmayer, and E. Nies, *Polymer Phase Diagrams: A Textbook*, Oxford University Press, NC, USA (2001).
5. R. A. Matkar, and T. Kyu, Phase diagrams of binary crystalline-crystalline polymer blends, *J. Phys. Chem. B*, **110**, 16059-16065 (2006).
6. D. Andelman, F. Brochard, and J. F. Joanny, Phase-transitions in Langmuir monolayers of polar-molecules, *J. Chem. Phys.*, **86**, 3673-3681 (1987).
7. D. Andelman, F. Brochard, C. Knobler, and F. Rondelez, In: W. M. Gelbart, A. Bhen-Shaul, and D. Roux (eds.). *Micelles, Membranes, Microemulsions, and Monolayers*, Springer-Verlag, Berlin, Germany (1994).
8. D. J. Keller, H. M. Mcconnell, and V. T. Moy, Theory of superstructures in lipid monolayer phase-transitions, *J. Phys. Chem.*, **90**, 2311-2315 (1986).
9. H. Mohwald, Phospholipid and phospholipid-protein monolayers at the air/water interface, *Annu. Rev. Phys. Chem.*, **41**, 441-476 (1990).
10. A. J. Dickstein, S. Erramilli, R. E. Goldstein, D. P. Jackson, and S. A. Langer, Labyrinthine pattern-formation in magnetic fluids, *Science*, **261**, 1012-1015 (1993).
11. R. E. Rosensweig, Magnetic Fluids, *Sci. Am.*, **247**, 124-132 (1982).
12. D. Vanderbilt, Phase segregation and work-function variations on metal-surfaces - spontaneous formation of periodic domain-structures, *Surf. Sci.*, **268**, L300-L304 (1992).
13. P. Zeppenfeld, M. Krzyzowski, C. Romainczyk, G. Comsa, and M. G. Lagally, Size relation for surface systems with long-range interactions, *Phys. Rev. Lett.*, **72**, 2737-2740 (1994).
14. L. Q. Chen, Phase-field models for microstructure evolution, *Annu. Rev. Mater. Res.*, **32**, 113-140 (2002).
15. G. L. Ge and L. Brus, Evidence for spinodal phase separation in two-dimensional nanocrystal self-assembly, *J. Phys. Chem. B*, **104**, 9573-9575 (2000).
16. E. Rabani, D. R. Reichman, P. L. Geissler, and L. E. Brus, Drying-mediated self-assembly of nanoparticles, *Nature*, **426**, 271-274 (2003).
17. U. Steiner, A. Meller, and J. Stavans, Entropy-driven phase-separation in binary emulsions, *Phys. Rev. Lett.*, **74**, 4750-4753 (1995).
18. A. Karim, T. M. Slawecki, S. K. Kumar, J. F. Douglas, S. K. Satija, C. C. Han, T. P. Russell, Y. Liu, R. Overney, O. Sokolov, and M. H. Rafailovich, Phase-separation-induced surface patterns in thin polymer blend films, *Macromolecules*, **31**, 857-862 (1998).
19. Z. Nie, A. Petukhova, and E. Kumacheva, Properties and emerging applications of self-assembled structures made from inorganic nanoparticles, *Nat. Nanotechnol.*, **5**, 15-25 (2010).
20. P. D. Yang and F. Kim, Langmuir-Blodgett assembly of one-dimensional nanostructures, *Chemphyschem.*, **3**, 503-506 (2002).
21. L. Cademartiri, K. J. M. Bishop, P. W. Snyder, and G. A. Ozin, Using shape for self-assembly, *Philos. T. R. Soc. A*, **370**, 2824-2847 (2012).
22. M. Brust, M. Walker, D. Bethell, D. J. Schiffrin, and R. Whyman, Synthesis of thiol-derivatized gold nanoparticles in a 2-phase liquid-liquid system, *J. Chem. Soc., Chem. Commun.*, 801-802 (1994).
23. J. R. Heath, C. M. Knobler, and D. V. Leff, Pressure/temperature phase diagrams and superlattices of organically functionalized metal nanocrystal monolayers: The influence of particle size, size distribution, and surface passivant, *J. Phys. Chem. B*, **101**, 189-197 (1997).
24. D. V. Leff, L. Brandt, and J. R. Heath, Synthesis and characterization of hydrophobic, organically-soluble gold nanocrystals functionalized with primary amines, *Langmuir*, **12**, 4723-4730 (1996).
25. D. V. Leff, P. C. Ohara, J. R. Heath, and W. M. Gelbart, Thermodynamic control of gold nanocrystal size - experiment and theory, *J. Phys. Chem.*, **99**, 7036-7041 (1995).
26. G. Markovich, D. V. Leff, S.-W. Chung, H. M. Soyez, B. Dunn, and J. R. Heath, Parallel fabrication and single-electron charging of devices based on ordered, two-dimensional phases of organically functionalized metal nanocrystals, *Appl. Phys. Lett.*, **70**, 3107-3109 (1997).
27. S.-W. Chung, G. Markovich, and J. R. Heath, Fabrication and alignment of wires in two dimensions, *J. Phys. Chem. B*, **102**, 6685-6687 (1998).
28. R. P. Sear, S.-W. Chung, G. Markovich, W. M. Gelbart, and J. R. Heath, Spontaneous patterning of quantum dots at the air-water interface, *Phys. Rev. E*, **59**, R6255-R6258 (1999).
29. P. C. Ohara, D. V. Leff, J. R. Heath, and W. M. Gelbart, Crystallization of opals from polydisperse nanoparticles, *Phys. Rev. Lett.*, **75**, 3466-3469 (1995).
30. V. S. Stubican and R. C. Bradt, Eutectic solidification in ceramic systems, *Annu. Rev. Mater. Sci.*, **11**, 267-297 (1981).
31. H. M. Mcconnell, Structures and transitions in lipid monolayers at the air-water-interface, *Annu. Rev. Phys. Chem.*, **42**, 171-195 (1991).
32. J.-F. Lemineur, N. Saci, and A. M. Ritcey, Impact of concentration and capping ligand length on the organization of metal nanoparticles in Langmuir-Blodgett surface micelles and nanostrands, *Colloids Surf. A: Physicochem. Eng. Asp.*, **498**, 88-97 (2016).
33. S.-W. Yeh, K.-H. Wei, Y.-S. Sun, U. S. Jeng, and K. S. Liang, CdS nanoparticles induce a morphological transformation of poly(styrene-b-4-vinylpyridine) from hexagonally packed cylinders to a lamellar structure, *Macromolecules*, **38**, 6559-6565 (2005).